Anatomy of a Polarization Switch of a Vertical-Cavity Semiconductor Laser

M. B. Willemsen, M. P. van Exter, and J. P. Woerdman
Huygens Laboratory, Leiden University, P.O. Box 9504, 2300 RA Leiden, The Netherlands
(Received 17 November 1999)

Using a streak camera we have measured the three Stokes polarization parameters during a polarization switch of a vertical-cavity semiconductor laser. The switch occurs along a corkscrew path on the Poincaré sphere and takes on average a few nanoseconds; this value agrees with a theoretical treatment based upon the Fokker-Planck equation.

PACS numbers: 42.65.Pc, 42.55.Px

The semiconductor vertical-cavity surface emitting laser (VCSEL) is the simplest conceivable microcavity laser, with a basically one-dimensional cavity matched to a single wavelength of light. VCSELs allow experimental study of basic issues in microlaser noise [1,2]. The small modal volume of a VCSEL results in strong spontaneous emission noise; in combination with the high degree of cylindrical symmetry, this leads to polarization switching between linear polarizations (x and y) [3]. In this Letter, we report a study of the *transient* aspects of polarization bistability of a VCSEL with a *single-shot* streak camera. Polarization bistability and switching in lasers in general, and VCSELs, in particular, are issues that have attracted a lot of attention over the years [3–8]. The most important quantity that has been studied experimentally so far is the residence time, i.e., the average time before a switch actually takes place [6,8]. However, the "jump" between the steady states has not been addressed directly, presumably because it occurs on a much faster time scale. Proper understanding of the switching route, which is generally embedded in a 3D state space (see below), requires *time-resolved* measurements.

To discuss our results we use the Poincaré sphere to represent all states of polarization (SOP). As spherical coordinates we introduce 2ϕ and 2χ, where ϕ corresponds to the polarization orientation and χ to the ellipticity. The equator corresponds to all linear SOP's, the poles to the two circular SOP's, and the rest to elliptical SOP's. The Cartesian axes of the Poincaré sphere are the normalized Stokes parameters, given by $s_1 = \cos(2\phi)\cos(2\chi)$, $s_2 = \sin(2\phi)\cos(2\chi)$, and $s_3 = \sin(2\chi)$, with $s_1^2 + s_2^2 + s_3^2 = 1$. Such a 3D display can be introduced for every two-mode system represented by two complex amplitudes.

Our theoretical framework is a rate-equation model, which is based upon an approximation of the quantum-well band structure of the VCSEL by discrete spin levels [9]. The spin-difference inversion can be eliminated adiabatically [10]; this procedure has been experimentally validated for practical VCSELs [11]. Furthermore, the fluctuations of the spin-averaged inversion and the total intensity are almost decoupled from the polarization fluctuations [9,12] and can be neglected in the present context. All this results in the following set of rate equations for the normalized Stokes parameters s_1, s_2, and s_3 [11]:

$$\frac{ds_1}{dt} = \gamma_\parallel(s_2^2 + s_3^2) + 2\omega_{\rm non}s_2s_3 + 2\gamma_{\rm non}s_1s_3^2 + f_{s_1}, \tag{1a}$$

$$\frac{ds_2}{dt} = -\gamma_\parallel s_1s_2 - \omega_{\rm lin}s_3 - 2\omega_{\rm non}s_1s_3 + 2\gamma_{\rm non}s_2s_3^2 + f_{s_2}, \tag{1b}$$

$$\frac{ds_3}{dt} = -\gamma_\parallel s_1s_3 + \omega_{\rm lin}s_2 - 2\gamma_{\rm non}s_3(s_1^2 + s_2^2) + f_{s_3}. \tag{1c}$$

The polarization dynamics is determined by dispersive anisotropies ($\omega_{\rm lin}$ and $\omega_{\rm non}$) and absorptive anisotropies ($\gamma_\parallel$ and $\gamma_{\rm non}$), which create a difference in frequency and gain between the two polarizations, respectively. Both anisotropies consist of a linear part ($\omega_{\rm lin}$ and $\gamma_\parallel$), which quantifies how much the cylindrical symmetry of the cavity is broken, and a nonlinear part ($\omega_{\rm non}$ and $\gamma_{\rm non}$), which corresponds to polarization-dependent saturation of the gain medium. The nonlinear anisotropies, which are remnants of the adiabatically eliminated spin-difference inversion, are the nonlinear birefringence $\omega_{\rm non} = \alpha\gamma_{\rm non}$ and the nonlinear dichroism $\gamma_{\rm non} = (\kappa/\Gamma)\mu$, where α is the amplitude-phase-coupling factor, κ the cavity decay rate, Γ the decay rate of the spin-difference inversion divided by that of the spin-averaged inversion, and μ is the normalized pump parameter [11]. Equations (1) describe the interplay between the stochastic Langevin forces ($f_{s_1}, f_{s_2}, f_{s_3}$) and the deterministic anisotropy forces, which drive the polarization back to its steady state.

In practical VCSELs $|\omega_{\rm lin}| \gg |\gamma_\parallel|, \omega_{\rm non}, \gamma_{\rm non}$ [11], so that the emitted light is either x or y polarized, depending on the sign of $\gamma_\parallel$ (for $\omega_{\rm lin} > 0$ and $\gamma_\parallel > 0$ the x polarization, i.e., $s_1 = 1$, has the highest eigenfrequency and highest modal gain). The fast $\omega_{\rm lin}$ rotation around the s_1 axis [see Eqs. (1b),(1c)] results in a rapid out-of-phase oscillation for s_2 and s_3 that can be averaged over in Eq. (1a), reducing the s_1 dynamics to a Kramers problem. Specifically, the second term in Eq. (1a) averages out (as $\langle s_2s_3\rangle \approx 0$) and the third term on the right-hand side (rhs), with $\langle s_3^2\rangle \approx (1 - s_1^2)/2$, acts as a symmetric Kramers double well potential, with minima at $s_1 = \pm 1$

and a barrier height $\gamma_{\rm non}/4$ at $s_1 = 0$. Previously it has been demonstrated that switches occur when $\gamma_{\parallel} \simeq 0$ [11,12], i.e., the first term on the rhs of Eq. (1a) is zero. In this case the VCSEL is bistable and switches stochastically between the x and y polarization [8]. We thus predict that during a polarization switch the s_1 Stokes parameter will gradually change from $s_1 = 1$ to $s_1 = -1$; this is the escape from one well to the other.

One may wonder if there is a different time duration of uphill paths (from $s_1 = 1$ to $s_1 = 0$), which are mainly stochastic, and downhill paths (from $s_1 = 0$ to $s_1 = -1$), which are mainly deterministic. For the calculation of the average transit time and in the experiment (see below) the probabilities of both paths are important. We have found that the various escapes obey a "stochastic inversion symmetry" around the potential maximum at $s_1 = 0$, in the sense that each uphill path has a mirror-imaged downhill path that is equally likely [13]. It is thus sufficient to consider only the downhill evolution. When we approximate the potential barrier around $s_1 = 0$ by an inverted parabola and use Ref. [14] we find that the conditional probability to find a value of s_1, assuming a start at $s_1 = 0$, is a Gaussian with a width that eventually increases exponentially in time. As the parabolic description is only valid close to $s_1 = 0$, we define the transit time $T_{\rm tr}$ as the time it takes to go from $s_1 = 1/2$ to $s_1 = -1/2$. The mean transit time $\langle T_{\rm tr} \rangle$, thus defined, is given by

$$\langle T_{\rm tr} \rangle \approx \frac{1}{\gamma_{\rm non}} \ln\left(\frac{\gamma_{\rm non}}{8D} + 1\right), \qquad (2)$$

where $\gamma_{\rm non}$ and D are proportional to the barrier height and spontaneous emission noise strength [with $\langle f_{s_i}(t) f_{s_i}(t + \tau)\rangle = 4D[1 - s_i^2]\delta(\tau)$].

Addressing now the s_2 and s_3 Stokes parameters, Eqs. (1b),(1c) predict that these parameters oscillate during the switch with a frequency $\approx \omega_{\rm lin}$ (in the case $\omega_{\rm lin} \gg \omega_{\rm non}, \gamma_{\rm non}$), leading to a "corkscrew" trajectory of the polarization switch (Fig. 1). A more detailed analysis shows that the $\omega_{\rm lin}$ rotation around the s_1 axis is perturbed by a $2\omega_{\rm non}$ rotation around the s_3 axis [see Eqs. (1a),(1b)], which is clockwise (cw) on the northern hemisphere and counterclockwise (ccw) on the southern hemisphere, resulting in the following expression for the frequency ω of the corkscrew oscillation during the switch:

$$\omega(s_1) \approx \omega_{\rm lin} + s_1 \omega_{\rm non}\,. \qquad (3)$$

The birefringence beat frequency is thus "dressed" with the nonlinear birefringence, arising from the spin dynamics. During the first part of the switch ($s_1 > 0$) the frequency ω is larger because the linear birefringence and nonlinear birefringence "cooperate," whereas they "cancel" during the second part of the switch ($s_1 < 0$).

For the experiments we have used a batch of 80 proton-implanted $Al_xGa_{1-x}As$ VCSELs with a 1λ cavity operating at 850 nm [11]. From this batch we selected the devices (10) that exhibited a polarization switch within the fundamental transverse mode regime. We used a single-shot streak camera (Hamamatsu M1952, S25 photo cathode) to measure the polarization in real time during the switch. The light emitted by the VCSEL is projected on a specific Stokes parameter by a $\lambda/4$ and a $\lambda/2$ wave plate, and an optical Faraday isolator.

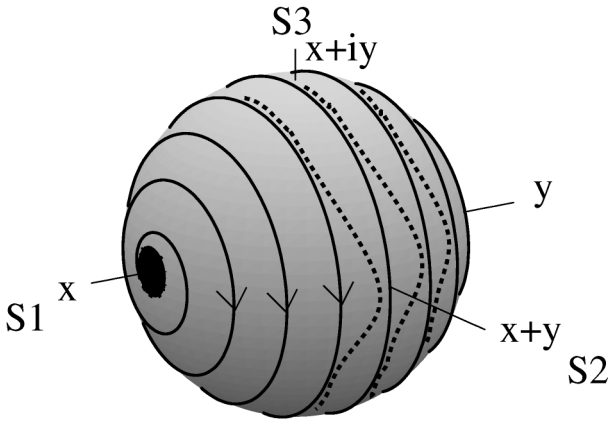

FIG. 1. The drawn curves show the corkscrew evolution of s_1, s_2, and s_3 on the Poincaré sphere during the polarization switch of a VCSEL. The dashed curves, which lie in the surface of the sphere, show the deformation of the circular orbits into a boomerang shape that occurs for VCSELs with very small, negative linear birefringence $\omega_{\rm lin}$.

We address now experimental results obtained from a typical VCSEL polarization switch within the range of fundamental transverse mode operation, the VCSEL being bistable at the switch current [8]. Measured time traces of subsequent polarization switches are shown in Fig. 2, where each time the polarization is projected on one of the Stokes parameters. The results clearly demonstrate the predicted corkscrew motion on the Poincaré sphere, as the polarization projection on s_1 shows a gradual increase whereas the projections on s_2 and s_3 show a transient oscillation. Note that the oscillation frequency in Fig. 2 indeed decreases during the switch as predicted by Eq. (3). To check this quantitatively, we determined $\omega_{\rm lin}$ and $\omega_{\rm non}$ independently with polarization homodyne detection [11], where we found a value of 2.1 and 0.55 GHz for $(\omega_{\rm lin}/2\pi)$ and $(\omega_{\rm non}/2\pi)$. This agrees with Fig. 2 and Eq. (3), as the frequency in the s_2/s_3 time traces indeed varies between the sum and difference of the quoted values of $\omega_{\rm lin}$ and $\omega_{\rm non}$.

The stochastic origin of the switches gives rise to a distribution of $T_{\rm tr}$ (see histogram in the inset of Fig. 2). The value of $T_{\rm tr}$ is determined from s_1 time traces by measuring the time interval [15] during which the intensity is between the 25% and 75% levels of the intensity after the switch (this criterion corresponds to $s_1 = +1/2 \rightarrow s_1 = -1/2$). On average no difference between uphill paths and downhill paths was observed, validating the stochastic inversion symmetry [13]. The mean value $\langle T_{\rm tr} \rangle$ was found to be 3.7(3) ns. To compare this with Eq. (2), we measured $\gamma_{\rm non}$ with polarization homodyne detection

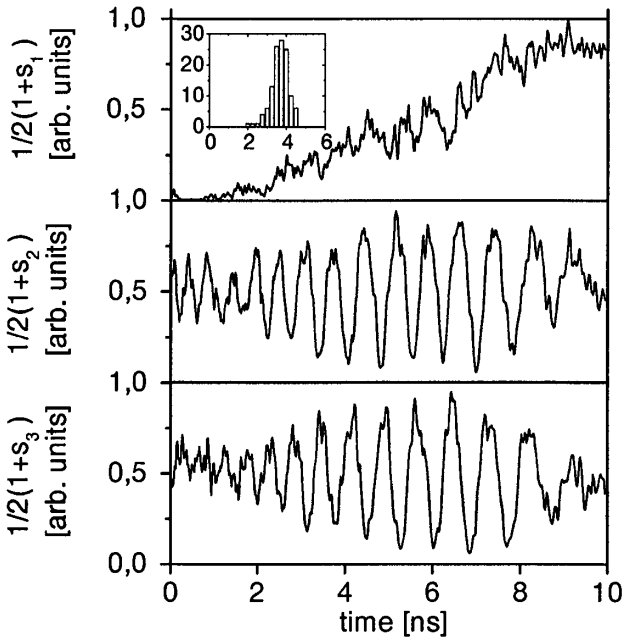

FIG. 2. Time-resolved measurements of the polarization during the switch. Each box shows the intensity projection on one of the Stokes parameters. The inset shows a distribution of transit times (ns), defined as the passage time from 25% to 75% in the $1/2[1 + s_1(t)]$ curve, obtained from 120 polarization switches of the same device.

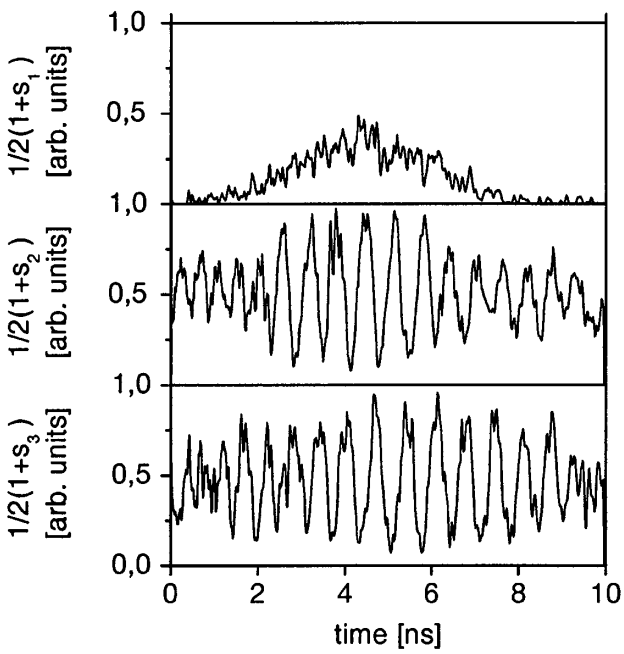

FIG. 3. Time-resolved measurements of a very large polarization fluctuation, where the size of the fluctuation is about half (in fact, 45%) of that of a complete polarization switch.

[11] and determined D from linewidth measurements with a self-heterodyne fiber-delay setup [8], resulting in a value of $\gamma_{\text{non}} \simeq 1.1(2)\ \text{ns}^{-1}$ and $D \simeq 7(1)\ \mu\text{s}^{-1}$ for this VCSEL. According to Eq. (2), this gives a value of $\langle T_{\text{tr}} \rangle \simeq 2.8(5)$ ns, which is in reasonable agreement with the directly measured value, which is expected to be somewhat larger anyhow due to the nonparabolic form of the potential farther away from the symmetry point.

Because of the stochastic nature of the problem, one must also expect events where the polarization makes a large excursion from its minimum in the potential (x or y polarized) but where the spontaneous emission noise is not strong enough to actually cross the barrier. A demonstration of such an event is shown in Fig. 3 (same laser as before), where the streak camera triggered on ≈45% of the level corresponding to a complete switch. The s_1 time trace shows that there is no switch, whereas the s_2/s_3 time traces still oscillate, as expected. A closer inspection of the s_2/s_3 traces confirms that the polarization did not switch, because there is no observable change in the oscillation period before and after the transient; the SOP stays on one side of the Poincaré sphere, $s_1 > 0$, [see Eq. (3)]. Figure 3 thus demonstrates that polarization fluctuations and switching have a common basis; after a polarization fluctuation the SOP spirals back to its steady state on the Poincaré equator.

When performing the measurements on different VCSELs, we generally found the same corkscrew scenario as discussed above. However, theory [4,11] predicts that switches at small negative ω_{lin} have a different nature. In this case the nonlinear birefringence ω_{non} can compensate the linear birefringence ω_{lin} so that the lasing and nonlasing polarization mode overlap in the optical spectrum, giving rise to a different switching mechanism. When $\omega_{\text{non}} \approx |\omega_{\text{lin}}|$, the ω_{non} rotation around the s_3 axis (being cw/ccw on the northern/southern hemisphere) has a dramatic effect on the ω_{lin} rotation, i.e., on the circular orbits around the s_1 axis. During the first part of this type of switch the deterministic orbits disappear effectively, whereas they appear during the second part, but heavily deformed into boomerang-shaped orbits (see the dashed curves in Fig. 1). These boomerang-shaped orbits should be visible as a "second harmonic" in the s_1 time trace as the bulges sketched in Fig. 1 also appear at the backside of the Poincaré sphere.

For experimental verification of this prediction we selected a rare VCSEL with very small birefringence $|\omega_{\text{lin}}/2\pi| \leq 0.5$ GHz. Figure 4 shows the time traces of the Stokes parameters during the switch for this rare VCSEL. The first part of the s_2/s_3 traces shows no oscillation, confirming that ω_{lin} and ω_{non} roughly cancel, whereas in the last part an oscillation appears as ω_{lin} and ω_{non} now add up. The deformation into boomerang orbits is demonstrated in the s_1 time trace of Fig. 4, which displays roughly double the frequency of the oscillations in the s_2/s_3 time traces.

Our work thus shows that the origin of a VCSEL polarization switch may be absorptive (Fig. 1) or dispersive (Fig. 4), as theoretically proposed [4]. We found experimentally that a dispersive switch has *two* conditions: a

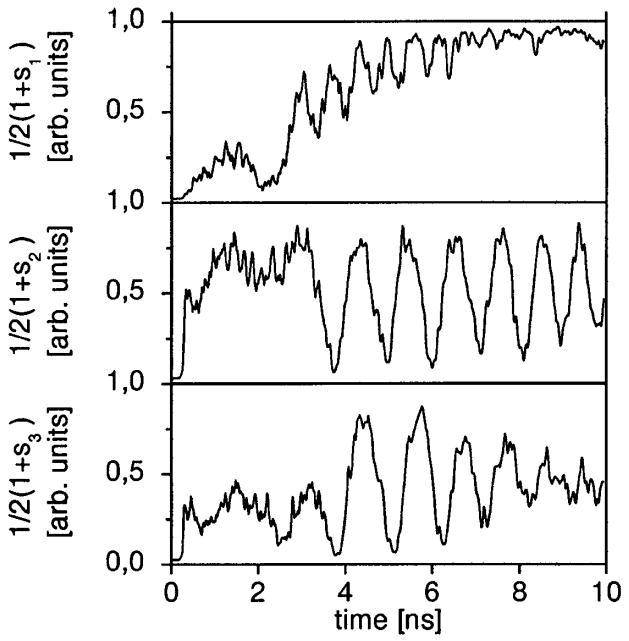

FIG. 4. Time-resolved measurements of a polarization switching VCSEL with extremely small, negative linear birefringence ($|\omega_{\text{lin}}/2\pi| \leq 0.5$ GHz). Note that for negative linear birefringence the frequency increases during the switch.

dispersive condition of small negative linear birefringence (ω_{lin}), as outlined above, as well as an absorptive condition of small linear dichroism ($\gamma_{\parallel}$). These two conditions are very rarely fulfilled: for practically all VCSELs $\omega_{\text{lin}} \gg \omega_{\text{non}}, \gamma_{\text{non}}$ and absorptive switching ($\gamma_{\parallel} \approx 0$) occurs.

In conclusion, we have addressed optical bistability in the transient regime by studying real-time polarization switching in VCSELs. The measurements, which are on a time scale that is generally not included in a Kramers description, agree with theory [11,14].

We acknowledge the experimental assistance of A. S. van de Nes, stimulating discussions with H. Dekker, and support from the FOM.

[1] D. C. Kilper, P. A. Roos, J. L. Carlsten, and K. L. Lear, Phys. Rev. A **55**, R3323 (1997).

[2] R. Jin, D. Boggavarapu, M. Sargent III, P. Meystre, H. M. Gibbs, and G. Khitrova, Phys. Rev. A **49**, 4038 (1994).

[3] K. D. Choquette, R. P. Schneider, Jr., K. L. Lear, and R. E. Leibenguth, IEEE J. Sel. Top. Quantum Electron. **1**, 661 (1995).

[4] J. Martín-Regalado, F. Prati, M. San Miguel, and N. B. Abraham, IEEE J. Quantum Electron. **33**, 765 (1997).

[5] J. Martín-Regalado, J. L. A. Chilla, J. J. Rocca, and P. Brusenbach, Appl. Phys. Lett. **70**, 3350 (1997); J. Martín-Regalado, S. Balle, and M. San Miguel, Opt. Lett. **22**, 460 (1997); B. Ryvkin *et al.*, J. Opt. Soc. Am. B **16**, 2106 (1999); S. Balle *et al.*, Opt. Lett. **24**, 1121 (1999).

[6] R. Roy, R. Short, J. Durnin, and L. Mandel, Phys. Rev. Lett. **45**, 1486 (1980); R. Roy and L. Mandel, Opt. Commun. **34**, 133 (1981).

[7] A. Le Floch, G. Ropars, J. M. Lenormand, and R. Le Naour, Phys. Rev. Lett. **52**, 918 (1984); G. Ropars, A. Le Floch, and R. Le Naour, Phys. Rev. A **46**, 623 (1992).

[8] M. B. Willemsen, M. U. F. Khalid, M. P. van Exter, and J. P. Woerdman, Phys. Rev. Lett. **82**, 4815 (1999).

[9] M. San Miguel, Q. Feng, and J. V. Moloney, Phys. Rev. A **52**, 1728 (1995).

[10] H. F. Hofmann and O. Hess, Quantum Semiclass. Opt. **10**, 87 (1998).

[11] M. P. van Exter, M. B. Willemsen, and J. P. Woerdman, Phys. Rev. A **58**, 4191 (1998).

[12] M. B. Willemsen, M. P. van Exter, and J. P. Woerdman, Phys. Rev. A **60**, 4105 (1999).

[13] The stochastic inversion symmetry is a consequence of the inversion symmetry of the stationary Kramers potential. It represents an extended form of detailed balance, which states that the joint probability to go from A to B in a certain time interval is equal to the joint probability to go from B to A [14], as the low conditional probability for an uphill path is compensated by the high probability to start at the bottom. Similarly, the high conditional probability for a downhill path is compensated by the low probability to start at the barrier.

[14] H. Risken, *The Fokker-Planck Equation* (Springer-Verlag, Berlin, 1996), Chap. 5.

[15] To determine the transit time T_{tr} from s_1 time traces, like Fig. 2a, we filtered the sharpest spikes by coarse-grain averaging and took average values in the case of multiple crossings of the 25% and 75% lines.